DNA tension-modulated translocation and loop extrusion by SMC complexes revealed by molecular dynamics simulations

Stefanos K. Nomidis,[1,2] Enrico Carlon,[1] Stephan Gruber,[3] and John F. Marko[4]

[1] *KU Leuven, Institute for Theoretical Physics, Celestijnenlaan 200D, 3001 Leuven, Belgium*
[2] *Flemish Institute for Technological Research (VITO), Boeretang 200, B-2400 Mol, Belgium*
[3] *Départment de Microbiologie Fondamentale, Université de Lausanne, 1015 Lausanne, Switzerland*
[4] *Department of Physics and Astronomy, and Department of Molecular Biosciences, Northwestern University, Evanston, Illinois 60208, USA*

(Dated: March 13, 2021)

Structural Maintenance of Chromosomes (SMC) protein complexes play essential roles in genome folding and organization across all domains of life. In order to determine how the activities of these large (about 50 nm) complexes are controlled by ATP binding and hydrolysis, we have developed a molecular dynamics (MD) model that realistically accounts for thermal conformational motions of SMC and DNA. The model SMCs make use of DNA flexibility and looping, together with an ATP-induced "power stroke", to capture and transport DNA segments, so as to robustly translocate along DNA. This process is sensitive to DNA tension: at low tension (about 0.1 pN), the model performs steps of roughly 60 nm size, while, at higher tension, a distinct inchworm-like translocation mode appears, with steps that depend on SMC arm flexibility. By permanently tethering DNA to an experimentally-observed additional binding site ("safety belt"), the same model performs loop extrusion. We find that the dependence of loop extrusion on DNA tension is remarkably different when DNA tension is fixed *vs.* when DNA end points are fixed: Loop extrusion reversal occurs above 0.5 pN for fixed tension, while loop extrusion stalling without reversal occurs at about 2 pN for fixed end points. Our model quantitatively matches recent experimental results on condensin and cohesin, and makes a number of clear predictions. Finally we investigate how specific structural changes affect the SMC function, which is testable in experiments on varied or mutant SMCs.

I. INTRODUCTION

Chromosomes in all living cells contain tremendously-long DNA molecules, ranging in size from megabases (millimeters) in bacteria and other microbes, to gigabases (meters) in some animals and plants. Many lines of evidence have long pointed to DNA or chromatin loop formation as a fundamental organizing principle of chromosome folding, and it has now become clear that the Structural Maintenance of Chromosomes (SMC) protein complexes are key drivers of DNA looping [1–3]. In the eukaryote case, condensin [4, 5] is thought to fold and compact chromosomes into first prophase and then metaphase chromatids via formation of tightly-packed tandem loops [6–8], while cohesin [9] is thought to actively generate gene-regulatory enhancer-promoter looping between CTCF sites [10, 11], as well as acting to hold sister chromatids together during mitosis [12, 13]. In bacteria, structurally-similar SMC complexes (SMCCs), notably bsSMC in *B. subtilis* [14, 15] and MukBEF in *E. coli* [16–18], act to fold chromosomes into highly-compacted, disentangled structures.

SMCCs are large and conformationally-flexible. They are based on dimers of SMC proteins, which have a distinctive 50-nm-long coiled-coil domain, terminated by a dimerization domain at one end and a Walker ATPase at the other. The two SMCs have their ATPase domains linked by a kleisin protein, hence forming a flexible, tripartite protein ring [19]. Experiments have established that *in vivo* DNA can be threaded through this protein ring [20–23], possibly aiding processivity of SMCC function along DNA. The latter may also depend on additional auxiliary proteins, which can, in general, bind near the ATPase-kleisin-ATPase junction.

The ATPase domains of the SMC protein dimer are thought to be linked together when ATP is bound, and unlinked following ATP hydrolysis. Thus, the ATP binding, hydrolysis and release cycle is coupled to large-scale conformational changes of the SMCC. It has been hypothesized [1, 2, 6, 7, 10, 11] that SMCCs are able to translocate along the DNA double helix (or along chromatin) in the manner of a molecular motor. Such a motor can perform active loop extrusion, *e.g.,* by simply binding to one spot on the DNA while translocating (thought to be the case for yeast condensin [24]). Indeed, a series of experiments have observed ATP-dependent DNA compaction by condensin [25–27], translocation by condensin [28], and loop extrusion by condensin [29] and cohesin [30–33]. However, the mechanism by which SMCCs perform these functions is unclear.

Here, we present a coarse-grained molecular dynamics (MD) model, which we believe provides a generic description of SMCC activities. It is based on prior analytical work on SMCC translocation and loop extrusion [34], but is able to take into account aspects of SMCC-DNA interactions which are difficult or impossible to deal with in a purely analytical framework, notably the synergy between conformational flexibilities of the SMC complex and the DNA it is moving along. The MD model is constructed from known features of SMCC/DNA interactions and the SMCC ATPase cycle, and contains enough detail to make a wide range of tests and predictions of

SMCC behavior.

The basic DNA-segment-capture mechanism [34] qualitatively explains existing experiments on SMCC translocation along DNA, but our MD model reveals new aspects of the model. We find that the flexibility of the SMC coiled-coils allows an alternative "inchworm" mode of translocation to come into play, when the underlying DNA is under too much tension to permit DNA segment bending to easily occur (roughly for DNA tension above 1 pN). Anchoring of the DNA to the SMCC during translocation gives rise to loop extrusion, and we find that existing experiments observing loop extrusion on DNAs anchored at two fixed points (thus at *fixed DNA extension*) are also readily described, with loop extrusion persisting up to tensions of about 2 pN. Remarkably, we also find that, if a similar experiment is carried out at *fixed DNA tension*, different mechanoenzyme behavior is observed, with true stalling followed by "loop de-extrusion", as force is increased beyond about 0.5 pN. Thanks to the role played by their distinctive structure in SMCC function, there are a number of conceivable modifications to SMCCs which should change their mechanical properties. We explore a few of these using our MD framework, predicting results for experiments on varied or mutated SMCCs.

II. RESULTS

A. MD model

1. Model geometry

The coarse-grained MD model is based on structural features common across SMCCs [34, 36]. It consists of individual rigid bodies (Fig. 1A), which interact through bond, angle and dihedral potentials (see Materials and Methods). Each of its two 50-nm-long coiled-coil arms consists of two straight segments, joined at a flexible "elbow" [37], which gives them the ability to open and close [36, 38]. The two SMCs are connected at the top by a dimerization "hinge" containing a DNA-binding locus [39–45]. The SMCs can also be connected at their Walker domain "heads", via two bound ATPs, and by a kleisin subunit [36]. The latter establishes the overall ring structure of the SMCC, and formation of the ATPase-ATP-ATPase "bridge" can divide the ring into two compartments [23, 46, 47].

We will refer to the DNA-binding sites of the hinge, ATP bridge and kleisin as *top*, *middle* and *bottom* binding sites, respectively (Fig. 1A, right). We make special note of the middle site at the bottom of the upper compartment, which requires ATP binding and engagement. This is a highly-conserved feature across SMCCs, and has been found to be essential for translocation in bsSMC [23, 47–51]. We use energetic binding to model SMCC-DNA interactions, but to some degree these sites, in particular the lower one, may sterically trap or embrace DNA [23, 47].

2. Structural states

The model SMCC has three distinct structural states, corresponding to the ATP-unbound (apo), ATP-bound, and ATP-hydrolyzed/ADP-bound states of the ATPase (Fig. 1B) [34]. In the *apo state* (0), the two arms and the upper compartment are closed, the ATP/ATPase bridge is open, the hinge DNA binding site is turned off and the lower compartment is folded by 45 degrees. In the *ATP-bound state* (1), which occurs upon ATP binding, the ATP bridge closes, the two arms open, and the lower compartment folds by an angle of 160 degrees. The opening of the arms makes the top DNA-binding site at the dimerization hinge accessible, which we model by turning on the top binding site of the open upper compartment. The same transition also activates the middle DNA-binding site, at the lower part of the compartment. Finally, in the *ADP-bound state* (2), the two arms remain open, the bottom and middle binding sites are turned off, the folding is reduced back to 45 degrees and the ATP bridge opens, and no longer separates the two compartments. Note that, the folding of the lower compartment is asymmetric, which is necessary for the motion of the SMCC to be directional.

3. Translocation mechanism

The SMCC translocates along DNA following a segment-capture mechanism [34], as illustrated in Fig. 1C. During a translocation cycle, it undergoes the transitions $0 \xrightarrow{k_{01}} 1 \xrightarrow{k_{12}} 2 \xrightarrow{k_{20}} 0$, where k_{01}, k_{12} and k_{20} are the respective rates. In this process, DNA starts out threaded through the lower compartment, bound at the bottom binding site. Upon transitioning to the ATP-bound state, the lower compartment folds, bringing DNA close to the middle binding site, to which it can efficiently bind (state 1a). This plays the role of a power stroke, as it forcibly pushes a DNA segment into the upper compartment. Subsequently, conformational fluctuations can lead distal DNA to bind to the upper binding site (state 1b), thus "capturing" a bent DNA segment (one could describe this captured segment as a small loop, but we will avoid that to better distinguish it from the larger, extruded DNA loops).

Following segment capture upon ATP hydrolysis, the ATPase bridge disintegrates, and conformational changes in the lower compartment lead to the middle and bottom binding sites being no longer active. Given that the DNA sequestration in the lower compartment may be due to steric trapping [23, 47], the release of DNA from the lower site could be a natural consequence of the opening of the bridge. With the bridge gone, the captured DNA segment can release bending stress by escaping through the

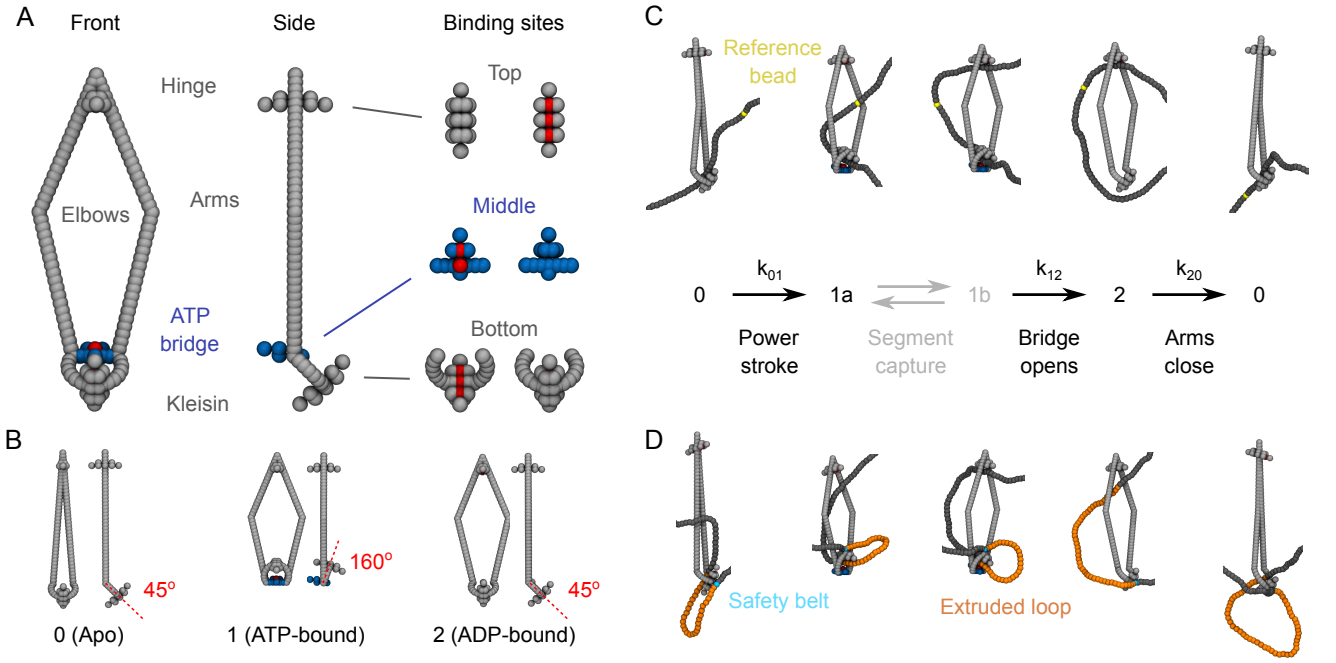

FIG. 1. Model details of the SMCC. (A) Geometry of the simulation model. For clarity, the top binding site, the ATP-bridge/middle-binding-site complex and the kleisin-subunit/lower-binding-site complex are also shown separately. The beads that are repulsive and attractive to DNA are shown in light gray and red color, respectively, while the repulsive ATP-bridge beads are indicated in blue. Note that, this SMCC configuration (open arms *and* kleisin at a 45-degree angle) is not an actual state of the model, but is rather used for illustration purposes. (B) Different structural states of the SMCC. Notice how the ATP bridge (blue) is absent (*i.e.,* the corresponding potential is set to zero) in the apo and ATP-bound states. (C) A single translocation cycle, following the mechanism proposed in Ref. 34. For reference, a fixed bead along the DNA track is indicated in yellow color. (D) A single loop extrusion cycle, according to the safety-belt mechanism. The extruded loop is indicated with orange color, while the tether point is marked with cyan. The visualization of the simulation snapshots was performed with VMD [35].

bottom of the complex. Finally, the SMCC returns to its apo state, with the closing of the two arms entropically pushing the DNA back to the now-reactivated bottom binding site. This sequence of states, ending with transport of the distal end of the captured segment from the top to the bottom of the SMCC protein loop, results in translocation of the SMCC along the DNA (indicated by the yellow reference DNA bead, Fig. 1C). Notably, in our MD model the SMCC transitions are entirely decoupled from DNA motion; it is possible for the segment capture process to fail, *i.e.,* for futile SMCC cycles to occur.

4. *Loop-extrusion mechanism*

Given translocation, loop extrusion may occur in a variety of ways [34, 52]. In this paper, we assume that a DNA segment (cyan bead in Fig. 1D) is attached to the exterior of the kleisin subunit, as is thought to be accomplished by the "safety belt" of yeast condensin [24]. Combined with the threading of DNA through the lower compartment, this leads to formation of a DNA loop. In this situation, translocation, as described above, leads to asymmetric loop extrusion, as the unattached end of the loop translocates along DNA. We note that, establishment of this mode of loop extrusion requires passage of the DNA through the SMC-kleisin protein ring (*topological loading*), possibly involving opening of a SMC-kleisin "gate" [51, 53]. We explore alternate loop-extrusion mechanisms compatible with our translocation model in Fig. 5 of the Discussion.

B. Translocation

We performed MD simulations for translocation of an SMCC along DNA under varying DNA tension, *i.e.,* with stretching force applied to the two DNA ends (see SI Appendix, Movies S1 and S2). Fig. 2A shows the observed translocation step size (blue points), averaged over many repeated cycles. As expected, the translocation slows down with increasing values of DNA tension, since it requires substantial bending of DNA (see Fig. 1C), which becomes progressively unfavorable as the latter gets stretched. Interestingly, the translocation of the SMCC does not halt at large DNA tensions, but instead reaches a plateau value of about 30 nm per cycle. This is due to the asymmetric folding of the lower compartment in the ATP-bound state, which may be viewed as a power stroke (state 1a in Fig. 1C), and is essentially un-

affected by the physiologically-relevant forces (< 10 pN) considered here.

We also measured the mean captured segment length in the ATP-bound state of the SMC complex (orange points in Fig. 2A). The data show a similar trend to the translocation steps, but are shifted to larger values by an approximately-constant distance. This indicates that DNA slippage occurs in the ADP-bound state, when the SMCC is not bound to DNA at all (transition $2 \rightarrow 0$ in Fig. 1C), by an amount essentially insensitive to DNA tension. The size of the captured segment is comparable to the persistence length of DNA (50 nm) and can be well described by a simple free-energy-minimization model (SI Appendix, Fig. S1).

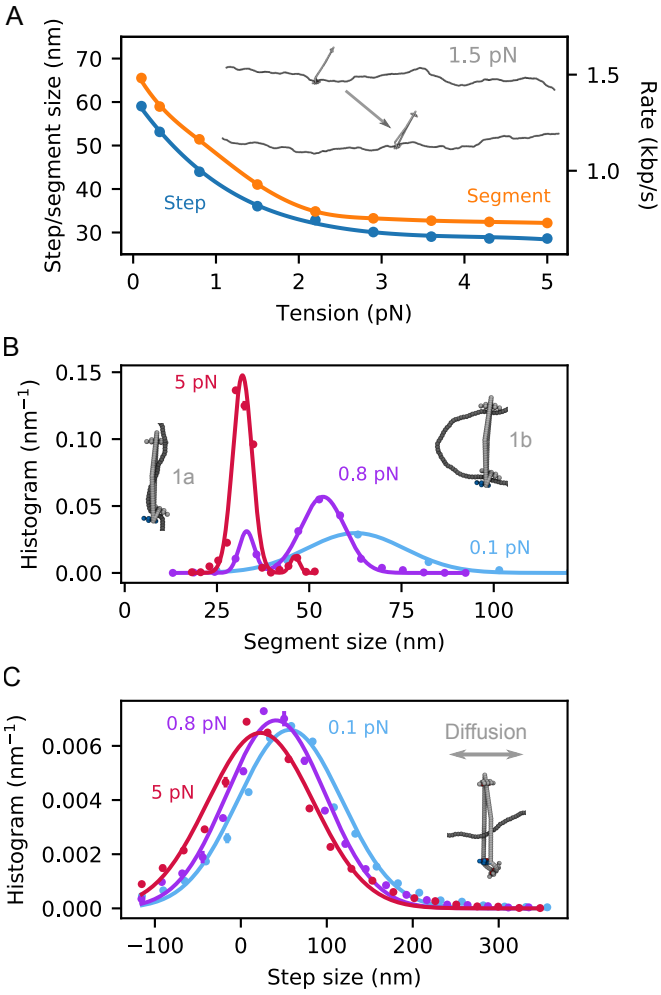

FIG. 2. DNA translocation by SMCC. (A) Mean step size (blue points) and captured segment length (ATP-bound state 1 in Fig. 1C, shown with orange points) dependence on DNA tension. Solid lines are spline interpolations, while the right axis converts the mean step size to translocation rate, using the conversion factor derived in Fig. 3. The inset shows the before-and-after configurations for a typical cycle at 1.5 pN. (B) Segment-size distribution for some selected tensions. The solid lines are single- and double-Gaussian fits to the data, while the vertical dashed line indicates the separation between substates 1a and 1b (see attached snapshots). (C) Step-size distribution for some selected tensions. Notice the difference in the length scale and width of the distributions between (B) and (C). This is a result of the SMCC diffusion, upon during the transition $2 \rightarrow 0$ (see attached snapshot).

Fig. 2B shows the distribution of capture-segment lengths in the ATP-bound state for a few values of DNA tension. We note the appearance of two distinct peaks at intermediate and high forces (*i.e.,* above about 0.2 pN). These peaks are indicative of two distinct substates, the relative population of which is tension dependent. The main distinction between the two substates is the attachment of a DNA segment to the top binding site (see snapshots), which is directly controlled by entropic fluctuations. The attached state is suppressed by high DNA tension, which favors state 1a over 1b. Movies S1 and S2 in SI Appendix show a typical translocation cycle at low and high DNA tension, respectively, and highlight this distinction.

For comparison, the respective distributions of the translocation step size are plotted in Fig. 2C, and appear to be substantially-wider than their ATP-bound captured segment counterparts, with a tension-independent spread. This suggests the existence of appreciable diffusion of the SMCC during the cycle, and in particular during the transition from the ADP-bound state back to the apo state (snapshot in Fig. 2C), when the SMCC is not directly attached to DNA. As a result, it can perform some backward steps (negative tails in Fig. 2C), but it still remains biased to execute directed motion on average. The translocation direction is solely determined by the orientation of the SMCC upon its topological loading, since the DNA track is left-right symmetric. The left-right symmetry, necessary for processive motor activity, is broken by the folding of the kleisin protein, and processively maintained by the topological linkage between the SMCC and the DNA (Fig. 1C).

C. Loop extrusion

Next, we investigated the loop extrusion process by the SMCC model, based on the safety-belt mechanism (Fig. 1D). We distinguish between two cases, depending on the origin of tension in DNA. In the first case, the tension is externally fixed, by applying a stretching force to the ends of the molecule. This can be realized with single-molecule micromanipulation techniques, such as optical or magnetic tweezers. In the second case, it is the end points of DNA that are externally fixed, which has been experimentally demonstrated *e.g.,* using DNAs attached at both ends to a surface [28–30]. As loop extrusion progresses, the nonextruded DNA is gradually stretched, leading to a corresponding increase in its tension.

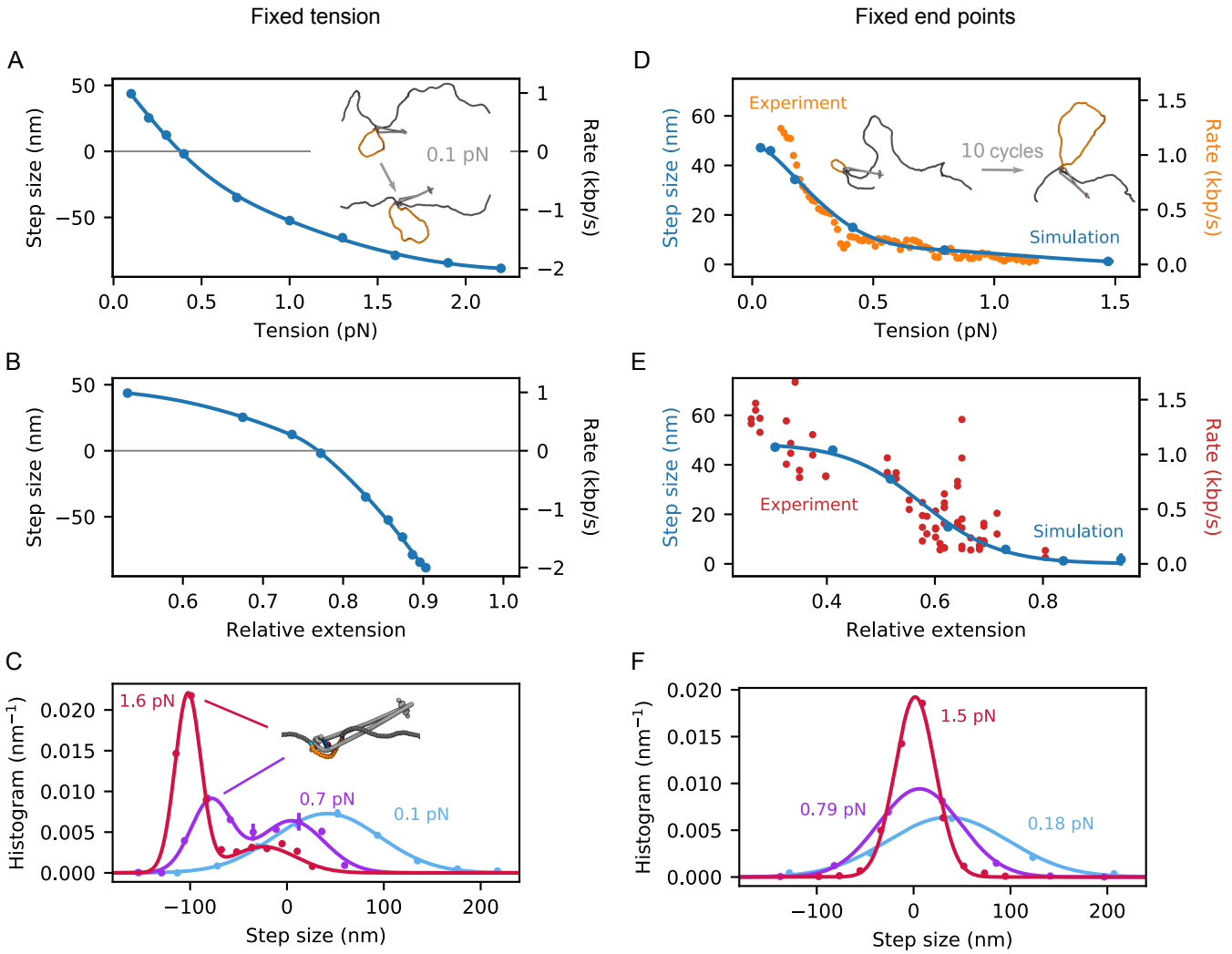

FIG. 3. Loop extrusion of DNA by an SMCC under fixed DNA tension (A-C) and end-point distance (D-F). (A) Loop extrusion step size as a function of DNA applied tension. The solid line is a spline interpolation of the simulation data (points). The inset shows the before-and-after configurations for a typical cycle at 0.1 pN. (B) Same data plotted against the corresponding mean relative extension. The solid line is again a spline interpolation of the simulation data (points). (C) Distribution of loop extrusion steps for some selected tensions. The solid lines are single- and double-Gaussian fits to the data (points). The attached snapshot is a representative configuration associated with the second peak at high tensions. (D) Loop extrusion step size as a function of the mean tension. The latter is computed from the mean net force exerted on the DNA ends. The solid line is a spline interpolation of the simulation data (blue points). For comparison, the experimental data of Ref. 29 are also shown with (orange points). The latter were originally obtained as a loop extrusion rate (right axis), so we transformed them into mean step size (left axis) by multiplying them with a factor of 44.2 s·nm/kbp, implying a cycle duration of 0.13 s. The inset shows some typical before-and-after configurations after the lapse of 10 cycles. (E) Same data plotted against the corresponding mean relative extension. The solid line is a fit of a logistic function. For comparison, the experimental data of Ref. 29 are also shown as red points. (F) Distribution of loop extrusion steps for some selected tensions. The solid lines are single-Gaussian fits to the data (points).

1. *Fixed tension*

Fig. 3A shows the mean loop extrusion step size, as a function of the applied tension. As expected, loop extrusion becomes less efficient with increasing DNA tension, similarly to the translocation process (Fig. 2A). In this case, however, the motor performs backward steps at large tension (above 0.4 pN), leading to a net shrinkage of the extruded loop. This takes place during the ADP-bound phase of the cycle (state 2 in Fig. 1D), during which the loop can exchange length with the rest of the DNA. Note that, these results were obtained for an initial loop size of 400 nm; the amount of slippage per cycle depends strongly on the loop size at the beginning of the cycle. A comparison among different initial loop sizes is shown in SI Appendix, Fig. S2B; for tensions be-

low stalling and slippage, the average step size converges with increasing initial loop size.

Fig. 3B shows the same data, as a function of the mean relative extension. The latter is computed using the known equilibrium relation between force and extension [54]. The step size distribution for some selected values of the tension is shown in Fig. 3C, and appears to be bimodal at high tensions. Analysis of the emergent second peaks reveals the presence of "imperfect cycles": The nontethered part of the DNA does not return to the bottom binding site at the end of the cycle, but instead remains in the upper compartment. This further exposes the loop to the external tension, leading to substantial loop shrinkage, *i.e.,* strongly-negative steps.

2. *Fixed end points*

Next, we performed molecular dynamics simulation of loop extrusion by fixing the end points of DNA. The latter started from a relative extension (*i.e.,* end-point distance divided by nonextruded DNA length) of 25%, while the attached SMCC performed a total of 10 loop-extrusion cycles per simulation run (see Movie S3 of SI Appendix). Fig. 3D shows the mean loop extrusion step size as a function of the average tension (blue points). This is obtained by a direct computation of the DNA tension after each cycle, and subsequent binning of the data. Note that, contrary to the fixed-tension case (Fig. 3A), fixing the end points puts a hard limit in the amount of DNA length that can be extruded, therefore loop extrusion halts at high tension (large extruded loops), without reversal. Note, finally, that the value of the mean step size at low tension (47 nm per cycle) is in quantitative agreement with that in the fixed-tension case (Fig. 3A).

Ganji et al. have experimentally measured the rate at which condensin extrudes loops in DNA with fixed end points, using a single-molecule assay [29]. Assuming a cycle duration of 0.13 s, we transformed the rates into steps per cycle (orange points in Fig. 3D) and plotted them alongside the simulation data, revealing a good agreement between the two. Fig. 3E shows data from the same simulations and experiments, plotted as functions of the relative DNA extension (end-to-end distance over nonextruded DNA length). There is good agreement between simulation and experiment, together with the gradual slowing of the motor at large DNA extension (high tension).

Fig. 3F shows the distribution of the mean loop extrusion step size for some selected mean tensions. In all cases, the data can be well fitted with a single Gaussian peak. Comparison between Figs. 3C and 3F further highlights the equivalence of the two setups, *i.e.,* fixed tension and end points, at low DNA tension/extension. Recent observations of step size distributions for yeast condensin [55] are in good agreement with our results.

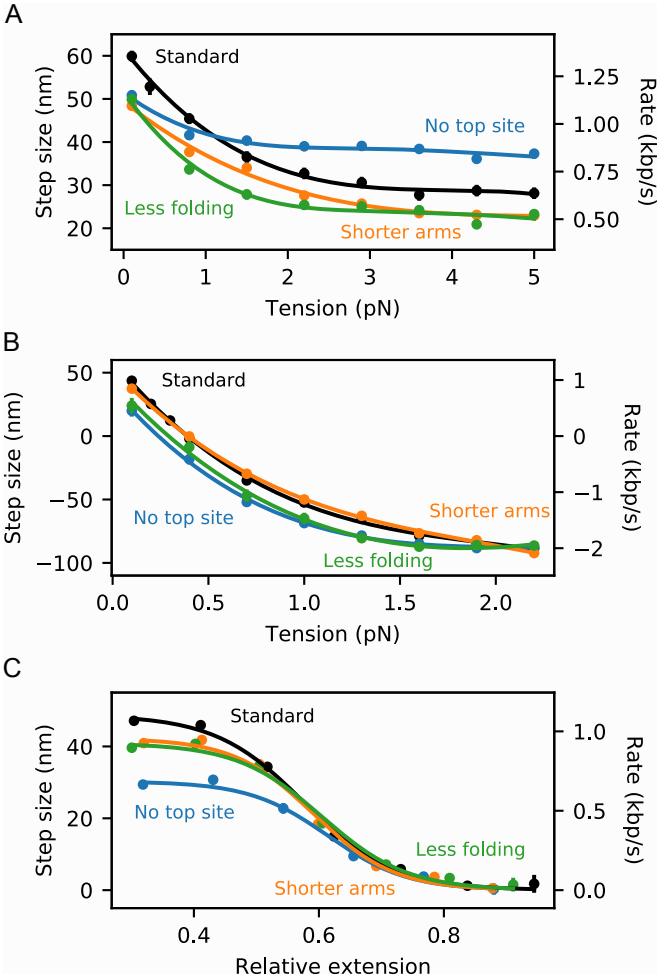

FIG. 4. Comparison among different sets of model parameters for (A) translocation, (B) loop extrusion under fixed tension and (C) loop extrusion under fixed end-point distance. The black points correspond to the parameters used throughout this work (standard), the blue points to a deactivation of the top binding site (no top site), the orange points to a shortening of the coiled-coil arms from 50 nm to 40 nm (shorter arms) and the green points to a reduction of the folding angle of the lower compartment in the ATP-bound state from 160 degrees to 130 degrees (less folding).

D. Varying the model parameters

In order to investigate how the behavior of the motor depends on the model details, we performed additional translocation, fixed-tension and fixed-end-points loop extrusion simulations for different model parameters (Fig. 4, panels A, B and C, respectively). More specifically, we deactivated the top binding site throughout the whole cycle, and found that the motor could still operate, suggesting that the existence of the top binding site is not a necessary element in the model (blue points). Interestingly, the translocation of the motor was found to be more efficient at high tension. This is likely due to the $2 \to 0$ transition being faster in that case, since

DNA needs to travel a shorter distance until it reaches the bottom binding site.

Additionally, we reduced the length of the coiled-coil arms from 50 nm down to 40 nm, and observed little to no difference (Fig. 4, orange points). We also reduced the folding angle of the lower compartment in the ATP-bound state from 160 to 130 degrees, which slightly slowed down the motor but did not keep it from translocating (green points). Finally, making the elbows in the SMC arms completely flexible (zero bending stiffness) did not keep translocation from occuring, although it proceeded via somewhat smaller steps at low force (Fig. S2A, SI Appendix). This emphasizes that conformational and mechanical details of the upper compartment are less important than the breaking of symmetry and topological separation of upper and lower compartments that occurs upon ATP binding. We conclude that the MD model motor function is qualitatively insensitive to a variety of modifications, and that it is likely applicable to a range of SMCCs. The quantitative predictions of the specific modifications we have examined amount to predictions for realizable SMCC mutation experiments.

III. DISCUSSION

The results presented above comprise a detailed analysis of the segment-capture model for SMC translocation and loop extrusion (Fig. 1) [34, 36]. The numerical nature of our model circumvents analytical limitations [34], and allows us to make a number of predictions for future experiments.

A. Translocation

Our model predicts the DNA-tension dependence of translocation by SMCCs (Fig. 2A), with the translocation rate dropping as DNA tension is increased through about 1 pN. Prior analytical modeling [34] did not fully explore the effect of a possible power stroke, in the form of kleisin folding. In our MD calculations, this allows translocation to proceed even when the DNA is tightly stretched, via an "inchworm"-like mechanism (smaller peak in captured segment size distribution, Fig. 2B). The drop to a plateau translocation rate with increasing force (Fig. 2A) is the signature of translocation occurring through two distinct mechanisms (two peaks in Fig. 2B), namely DNA bending and segment capture at lower forces *vs.* "inchworming" (possibly involving SMC bending) at high forces.

To date, no translocation experiments at controlled tension have been carried out. Observation of translocation by yeast condensin observed a velocity of 60 bp/s for DNA tension estimated to be 0.3 pN [28]. This is substantially slower than the respective estimate of about 1.2 kbp/s from our MD model (Fig. 2A), the cycling rate of which was set using loop-extrusion experiments [29]. This deviation may, thus, reflect a large variability in the motor efficiency, depending on the precise experimental conditions.

In addition to the tension-velocity behavior, the MD model makes clear predictions for the size distribution of the DNA segment capture (Fig. 2B) (which, for the inchworm mode, corresponds to essentially the length of the SMCC), as well as for the translocation step (Fig. 2C). The model shows that the relatively-narrow captured DNA segment size is broadened by diffusion into a more smeared-out DNA step size distribution. The smearing is a result of the entropic transport of DNA from the top binding site back to the bottom one following ATP hydrolysis (Fig. 1C), during which diffusion of the SMCC along the DNA can freely occur. Cohesin has been observed to diffuse on DNA [56] in experiments lacking the motor-processivity protein NIPBL [30].

The model's key transition, which breaks left-right symmetry and provides a power stroke, is head engagement and folding of the lower compartment (Fig. 1B), guiding the DNA to the middle binding site on top of the Walker ATPase heads (Fig. 1C). This leads to formation of a DNA segment in the upper compartment ($0 \rightarrow 1a \rightarrow 1b$ in Fig. 1C). A remarkable result is that the top binding site is dispensable, in that translocation and loop extrusion persist without it (Fig. 4A-C, blue curves). In accord with this, a recent genetic experiment on bsSMC mutated away putative DNA-binding residues in the upper "hinge" domain, with little effect on translocation and loop extrusion *in vivo* [23].

Our observation of a lack of necessity for the upper-compartment DNA-binding sites may help to explain the variability in the hinge-proximal DNA-binding across SMCCs. While the presence of a positively-charged "channel" (with, so far, poorly-understood function) along with a positively-charged surface on the hinge are conserved [42], the precise location of basic residues on the hinge surface varies appreciably across SMCCs [40, 41, 44, 45]. This variability may reflect our result that the top binding site is not crucial, and is involved in fine-tuning of SMCC function. Our model enzyme cycle does require DNA release from the top site following arm refolding, and we can expect the top site to be relatively weak, so as to have its interaction with DNA disrupted by the return to the apo state.

Current experiments and Fig. 2 do not consider the effect of a load force, examining DNA translocation only as a function of DNA tension. It would be informative to additionally apply a direct load to the enzyme, and to examine translocation velocity as a function of both DNA tension and enzyme load force. This could be realized with a combination of three applied forces using, *e.g.,* triple force-controlled optical tweezers, with forces f_{tension} and $f_{\mathrm{tension}} - f_{\mathrm{load}}$ at the two ends of the DNA, and f_{load} applied to the SMCC [34]. A recent study observed translocation for cohesin at a velocity of 0.4 kbp/s against a buffer flow [30]. The latter may introduce both DNA tension (by stretching) and a load force

on the SMCC, although in an imperfectly-quantitatively-controlled fashion.

B. Loop extrusion: fixed end points *vs.* fixed tension

The MD model quantitatively describes compaction rates observed in experiments on loop extrusion at fixed DNA end-point distance [29] (Fig. 3D,E), and additionally predicts step sizes and their distributions (Fig. 3F). The tension in the DNA builds up as a loop is extruded, and there comes a point at which the enzyme stalls. Due to this externally-induced tension-extrusion coupling, the loop can never shrink, and thus the MD rate *vs.* tension is always positive, asymptotically approaching zero for large forces, as observed experimentally (Fig. 3D,E).

The positivity of compaction rate with fixed end points is in stark contrast to the situation for fixed DNA tension, where there is a well-defined stall tension, beyond which an initially-extruded loop will start shrinking (Fig. 3A,B). Indeed, our MD model is eventually forced to run in reverse, taking negative steps of well-defined size (Fig. 3C). Evidence for reversal of SMCC loop extrusion/translocation by force exists, in the form of Hi-C data from *B. subtilis* consistent with bsSMC-RNAP collisions forcing bsSMC backwards along DNA [57]. Experiments on loop extrusion *vs.* controlled DNA tension would provide further insight into how SMCCs on DNA can be pushed around by other enzymes. *In vivo* one can imagine loop extrusion being opposed by both fixed endpoint and fixed tension restraints, the former being relevant to a chromosomal domain, which is defined by binding to solid cellular structures at two distant points, and the latter being relevant to molecular motors, such as polymerases, which might act to generate tension in a DNA segment.

C. Head engagement power stroke

In the MD model, ATP binding and head engagement are associated with a conformational change of the SMCC, which facilitates segment capture from one side of the enzyme (Fig. 1B,C). Such a symmetry-breaking event is necessary for the translocation to be directional, otherwise DNA segments would be captured with equal efficiency from both directions, and the enzyme would move randomly left and right along its unpolarized DNA track. This conformational change might be directly observable in an experiment that monitors the enzyme itself, *e.g.,* by monitoring the distance between ATPase heads directly, or the effect of head engagement on overall conformation of the enzyme.

In our SMCC model, head engagement and kleisin folding move the lower edge of the enzyme by a distance of roughly 10 nm (vertical distance moved by lower edge between states 0 and 1 in Fig. 1B). In our model, this transition can actually be observed in terms of a small contraction in the flanking DNA (Fig. S3, SI Appendix), although to actually observe this it is likely that a quite short DNA will have to be used (our MD calculations use a total of 1.5 kb).

By applying sufficient force against this conformational change, one might be able to keep it from occurring, providing measurement of the enzyme power stroke. The threshold to overpower the conformational change would likely be a force in the vicinity of 10 pN, *i.e.,* the force scale associated with breaking noncovalent biomolecule-biomolecule interactions, or the stalling of molecular motors. Note that, such a stall force for translocation is not directly related to that for loop extrusion (Fig. 2A *vs.* Fig. 3D). We finally note that recent observations of large ATP-hydrolysis-independent contractions of SMCC-DNA complexes [55] are likely looking at the DNA segment capture process rather than protein conformational change.

D. SMC coiled-coil conformation and flexibility

A feature of the model that we have explored is the effect of SMC coiled-coil "arm" flexibility on SMCC translocation and loop extrusion. We have found that making SMC arm joints completely flexible does not abrogate translocation (Fig. S2A, SI Appendix), and in fact eliminates the need for DNA bending, thus likely facilitating translocation at high DNA tensions. This may be important, given that there are observations of rather extreme SMC arm flexibility for condensin [58, 59], although recent cryo-EM images of precisely the same type of condensin [60] suggest conformational properties similar to what we have assumed here. However, essentially the same motor function should result from variations on the protein-ring closure mechanism presumed here, for example an ATP-dependent "collapse" of the protein ring [55].

The main features needed for SMCCs to translocate in the manner described by our model are the folding/breaking of symmetry in the lower compartment, and the formation of separated upper and lower compartments, both a result of ATP binding. We have found that DNA binding interactions, apart from some mechanism to hold on to DNA in the lower compartment, are largely dispensable. The key elements of our model are largely topological: passage of DNA through the protein ring, and the ATP-dependent division of the ring into upper and lower compartments. Models of SMC function which do not incorporate the topological nature of SMCC-DNA interaction will have weak directional processivity due to the left-right symmetry of duplex DNA.

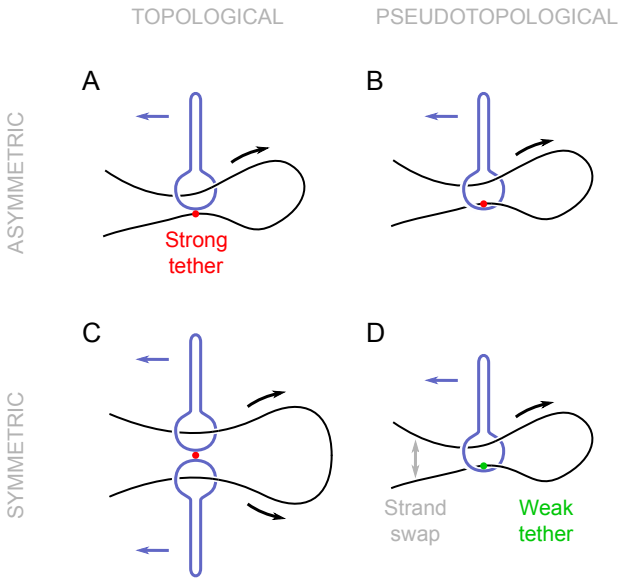

FIG. 5. Different loop extrusion mechanisms, categorized according to loading mechanism (vertical) and symmetry of loop extrusion (horizontal). (A) Permanently attaching DNA to the exterior of the SMCC (safety belt, marked with red) leads to asymmetric loop extrusion. This requires DNA threading through the lower compartment, and is the mechanism used in this work. (B) Moving the tethering point to the interior of the SMCC does not require opening of the protein ring, but rather an insertion of a DNA hairpin. (C) Two permanently-joined SMCCs translocating in opposite directions can symmetrically extrude loops. (D) If the tether in the interior of the SMCC is weak, such that DNA detachment and strand swap can take place, the same pseudotopological model as in (B) can now symmetrically extrude loops.

E. Loading topology and symmetry of loop extrusion

As discussed earlier, translocation is the fundamental function of SMCCs that underlies all modes of loop extrusion. Depending on the SMCC, it appears that different modes do occur, with distinct loading mechanisms and symmetry of loop extrusion (Fig. 5). For example, it has been suggested that yeast condensin translocation and loop extrusion require passage of the DNA through a transient opening of the SMCC protein ring [26]. For this SMCC, the apparent anchoring of the DNA to the outside of the ring (safety belt) requires topological loading, and leads to asymmetric loop extrusion (Fig. 5A), formally the mode used in our MD model.

In principle, our MD model may also be applied to the case where the DNA is bound *inside* the SMC-kleisin ring (Fig. 5B). While this is geometrically identical to the external safety-belt scheme (the relocation of the tethered DNA strand from the outside to the inside of the kleisin is inconsequential to the cycle of Fig. 1D), there is a key topological difference: no opening of the protein ring is required to initiate the loop-extrusion process, since the DNA can be bent into a hairpin and then inserted into the SMC-kleisin ring (*pseudotopological loading*) [34]. As long as DNA remains tethered in the interior of the SMC-kleisin ring, this mechanism generates one-sided, asymmetric loop extrusion, similar to the external safety belt.

A third possibility is a simple variation of the above, where the tethering of DNA is weak enough to allow transient detachment and reattachment (Fig. 5D). Since two DNA segments are in close proximity in the interior of the SMCC protein loop, a strand swap can take place, possibly via facilitated dissociation (likely a strong effect under the strong confinement of two DNA strands in the SMCC lower compartment) [61]. If this occurs relatively slowly compared to the cycling time, the result will be progressive extrusion on both sides of the loop *i.e.,* symmetric pseudotopological loop extrusion, as indeed has been observed for cohesin [30]. Each strand swap event translates to a change in which side of the loop DNA segments are captured from, which might be detectable given sufficient temporal resolution.

Finally, a fourth possible "dimerized translocator" can result from the coupling of two SMCCs together (Fig. 5C), each translocating to an opposite direction, so as to accomplish symmetric loop extrusion at double the velocity of a single translocator [34]. This scenario requires topological loading of DNA segments into both of the dimerized SMC-kleisin rings. Evidence exists for dimerization of the *E. coli* SMCC MukBEF *in vivo* [62–64], as well as for ATP-dependent compaction activity by oligomerized condensins *in vitro* [27, 31].

This suggests a rule: single SMCCs that require topological loading *must* asymmetrically extrude loops (at least between successive protein-loop-opening events), while ones that load pseudotopologically *can* perform symmetric loop extrusion (cohesin). A recent study indicates that condensin from metaphase *Xenopus* egg extracts drives more asymmetric loop extrusion than does cohesin from interphase extracts [32], consistent with condensin being topologically loaded, and (interphase) cohesin being pseudotopologically loaded. The precise rules for how loading and loop extrusion occur *in vivo* are likely regulated by factors that mediate SMCC protein loop opening [47, 51].

IV. MATERIALS AND METHODS

A. MD

All simulations were performed in LAMMPS [65], using a standard velocity-Verlet integration scheme coupled to a Langevin thermostat. The simulation temperature was 300 K, with a damping parameter of 0.5 ns, while the simulation timestep was 0.2 ps.

B. DNA

DNA was modeled as a semiflexible bead-and-spring polymer (dark gray beads in Fig. 1C,D). Each bead represented 5 bp with a mass of 0.017 ag (10 kDa), while successive beads were connected through finitely-extensible springs, with a rest length of 1.7 nm. The DNA stiffness was modeled through angle interactions among three successive beads, yielding a persistence length of 50 nm. Excluded-volume interactions were taken into account by means of truncated and shifted Lennard-Jones interactions, with an interaction distance of 3.5 nm, *i.e.,* the effective DNA diameter at physiological salt conditions [66]. A total of 301 beads were used, corresponding to a 1.5-kbp sequence with a contour length of 510 nm.

C. SMCC

The SMCC consisted of 7 rigid bodies (Fig. 1A): four coiled-coil segments, the top binding site, the ATP bridge together with the middle binding site, and the kleisin subunit together with the bottom binding site. These interacted with each other by means of bond, angle and dihedral potentials. Each bead had a diameter 1.5 nm, and the total mass of the SMCC was chosen to be 0.25 ag (150 kDa). The coiled-coil arms were made of two connected, 25-nm-long, straight segments, interacting through a harmonic angle potential of 30 $k_{\mathrm{B}}T/\mathrm{rad}^2$ stiffness. The upper binding site consisted of a total of 17 beads. Three of these were chosen to be attractive to DNA (red beads), while the rest of them were repulsive (light gray beads). This ensured that DNA could only bind from a single direction. The ATP bridge was made of 2 attractive (red) and 6 repulsive beads (blue) attached to a 7.5-nm-long, straight segment (blue). The kleisin subunit consisted of 3 attractive (red) and 14 repulsive beads (light gray) attached to a circular arc of radius 7 nm (light gray). The top binding site, the ATP bridge and the kleisin subunit were kept aligned by means of bond and dihedral interactions. The attraction of DNA by the binding sites was modeled with a truncated and shifted Lennard-Jones interaction, with a potential depth of 3.2 $k_{\mathrm{B}}T$ for each top- and middle-binding-site bead, and 11 $k_{\mathrm{B}}T$ for the bottom-site beads. In order to control the angle between the ATP bridge and the lower half of each arm, harmonic angle potentials were used, with a stiffness of 100 $k_{\mathrm{B}}T/\mathrm{rad}^2$. The two arms were made bendable by introducing similar harmonic angle potentials, with a stiffness of 30 $k_{\mathrm{B}}T/\mathrm{rad}^2$. The asymmetric folding of the kleisin subunit was achieved through two harmonic dihedral interactions, with stiffness constants of 60 $k_{\mathrm{B}}T/\mathrm{rad}^2$ and 100 $k_{\mathrm{B}}T/\mathrm{rad}^2$. The SMCC cycled stochastically through the three different states, apo (0), ATP-bound (1) and ADP-bound (2), with mean dwell times of $\tau_{01} = 0.4$ μs, $\tau_{12} = 1.6$ μs and $\tau_{20} = 0.4$ μs in simulation time units. Instantaneous dwell times were drawn from exponential distributions. For the determination of the loop size in Fig. 2, we identified where the upper SMCC compartment encircled DNA. In particular, we located the DNA bead closest to the center of mass of the upper compartment, and also the one closest to the top binding site, and compared the two distances. This determined whether the system was in state 1a or 1b, *i.e.,* DNA was closer to the center of mass or the top binding site, respectively (see also Fig. 1C). The loop end was associated with the smallest-proximity DNA bead.

[1] K. Nasmyth, Disseminating the genome: joining, resolving, and separating sister chromatids during mitosis and meiosis, Annu. Rev. Genet. **35**, 673 (2001).

[2] E. Alipour and J. F. Marko, Self-organization of domain structures by DNA-loop-extruding enzymes, Nucleic Acids Res. **40**, 11202 (2012).

[3] S. Datta, L. Lecomte, and C. H. Haering, Structural insights into DNA loop extrusion by SMC protein complexes, Curr. Opin. Struct. Biol. **65**, 102 (2020).

[4] T. Hirano and T. J. Mitchison, A heterodimeric coiled-coil protein required for mitotic chromosome condensation in vitro, Cell **79**, 449 (1994).

[5] A. V. Strunnikov, E. Hogan, and D. Koshland, SMC2, a Saccharomyces cerevisiae gene essential for chromosome segregation and condensation, defines a subgroup within the SMC family, Genes Dev. **9**, 587 (1995).

[6] A. Goloborodko, J. F. Marko, and L. A. Mirny, Chromosome compaction by active loop extrusion, Biophys. J. **110**, 2162 (2016).

[7] A. Goloborodko, M. V. Imakaev, J. F. Marko, and L. Mirny, Compaction and segregation of sister chromatids via active loop extrusion, eLife **5**, e14864 (2016).

[8] J. H. Gibcus, K. Samejima, A. Goloborodko, I. Samejima, N. Naumova, J. Nuebler, M. T. Kanemaki, L. Xie, J. R. Paulson, W. C. Earnshaw, L. A. Mirny, and J. Dekker, A pathway for mitotic chromosome formation, Science **359** (2018).

[9] A. V. Strunnikov, V. L. Larionov, and D. Koshland, SMC1: an essential yeast gene encoding a putative head-rod-tail protein is required for nuclear division and defines a new ubiquitous protein family, J. Cell Biol. **123**, 1635 (1993).

[10] A. L. Sanborn, S. S. Rao, S.-C. Huang, N. C. Durand, M. H. Huntley, A. I. Jewett, I. D. Bochkov, D. Chinnappan, A. Cutkosky, J. Li, *et al.*, Chromatin extrusion explains key features of loop and domain formation in wild-type and engineered genomes, Proc. Natl. Acad. Sci. U.S.A. **112**, E6456 (2015).

[11] G. Fudenberg, M. Imakaev, C. Lu, A. Goloborodko, N. Abdennur, and L. A. Mirny, Formation of chromosomal domains by loop extrusion, Cell Rep. **15**, 2038 (2016).

[12] V. Guacci, D. Koshland, and A. Strunnikov, A direct link between sister chromatid cohesion and chromosome

condensation revealed through the analysis of MCD1 in S. cerevisiae, Cell **91**, 47 (1997).

[13] C. Michaelis, R. Ciosk, and K. Nasmyth, Cohesins: chromosomal proteins that prevent premature separation of sister chromatids, Cell **91**, 35 (1997).

[14] M. Hirano and T. Hirano, ATP-dependent aggregation of single-stranded DNA by a bacterial SMC homodimer, EMBO J. **17**, 7139 (1998).

[15] X. Wang, H. B. Brandão, T. B. Le, M. T. Laub, and D. Z. Rudner, Bacillus subtilis SMC complexes juxtapose chromosome arms as they travel from origin to terminus, Science **355**, 524 (2017).

[16] H. Niki, A. Jaffe, R. Imamura, T. Ogura, and S. Hiraga, The new gene mukB codes for a 177 kd protein with coiled-coil domains involved in chromosome partitioning of E. coli., EMBO J. **10**, 183 (1991).

[17] V. S. Lioy, A. Cournac, M. Marbouty, S. Duigou, J. Mozziconacci, O. Espéli, F. Boccard, and R. Koszul, Multiscale structuring of the E. coli chromosome by nucleoid-associated and condensin proteins, Cell **172**, 771 (2018).

[18] J. Mäkelä and D. J. Sherratt, Organization of the escherichia coli chromosome by a MukBEF axial core, Mol. Cell **78**, 250 (2020).

[19] T. Hirano, Condensin-Based Chromosome Organization from Bacteria to Vertebrates, Cell **164**, 847 (2016).

[20] C. H. Haering, A. M. Farcas, P. Arumugam, J. Metson, and K. Nasmyth, The cohesin ring concatenates sister DNA molecules, Nature **454**, 297 (2008).

[21] S. Cuylen, J. Metz, and C. H. Haering, Condensin structures chromosomal DNA through topological links, Nat. Struct. Mol. Biol. **18**, 894 (2011).

[22] L. Wilhelm, F. Bürmann, A. Minnen, H. C. Shin, C. P. Toseland, B. H. Oh, and S. Gruber, SMC condensin entraps chromosomal DNA by an ATP hydrolysis dependent loading mechanism in Bacillus subtilis, Elife **4** (2015).

[23] R. V. Nunez, L. B. R. Avila, and S. Gruber, Transient DNA occupancy of the SMC interarm space in prokaryotic condensin, Mol. Cell **75**, 209 (2019).

[24] M. Kschonsak, F. Merkel, S. Bisht, J. Metz, V. Rybin, M. Hassler, and C. H. Haering, Structural basis for a safety-belt mechanism that anchors condensin to chromosomes, Cell **171**, 588 (2017).

[25] T. R. Strick, T. Kawaguchi, and T. Hirano, Real-time detection of single-molecule DNA compaction by condensin I, Curr. Biol. **14**, 874 (2004).

[26] J. M. Eeftens, S. Bisht, J. Kerssemakers, M. Kschonsak, C. H. Haering, and C. Dekker, Real-time detection of condensin-driven DNA compaction reveals a multistep binding mechanism, EMBO J. **36**, 3448 (2017).

[27] R. A. Keenholtz, T. Dhanaraman, R. Palou, J. Yu, D. D'Amours, and J. F. Marko, Oligomerization and ATP stimulate condensin-mediated DNA compaction, Sci. Rep. **7**, 14279 (2017).

[28] T. Terakawa, S. Bisht, J. M. Eeftens, C. Dekker, C. H. Haering, and E. C. Greene, The condensin complex is a mechanochemical motor that translocates along DNA, Science **358**, 672 (2017).

[29] M. Ganji, I. A. Shaltiel, S. Bisht, E. Kim, A. Kalichava, C. H. Haering, and C. Dekker, Real-time imaging of DNA loop extrusion by condensin, Science **360**, 102 (2018).

[30] I. F. Davidson, B. Bauer, D. Goetz, W. Tang, G. Wutz, and J. M. Peters, DNA loop extrusion by human cohesin, Science **366**, 1338 (2019).

[31] Y. Kim, Z. Shi, H. Zhang, I. J. Finkelstein, and H. Yu, Human cohesin compacts DNA by loop extrusion, Science **366**, 1345 (2019).

[32] S. Golfier, T. Quail, H. Kimura, and J. Brugués, Cohesin and condensin extrude DNA loops in a cell cycle-dependent manner, Elife **9** (2020).

[33] M. Kong, E. E. Cutts, D. Pan, F. Beuron, T. Kaliyappan, C. Xue, E. P. Morris, A. Musacchio, A. Vannini, and E. C. Greene, Human Condensin I and II Drive Extensive ATP-Dependent Compaction of Nucleosome-Bound DNA, Mol. Cell **79**, 99 (2020).

[34] J. F. Marko, P. De Los Rios, A. Barducci, and S. Gruber, DNA-segment-capture model for loop extrusion by structural maintenance of chromosome (SMC) protein complexes, Nucleic Acids Res. **47**, 6956 (2019).

[35] W. Humphrey, A. Dalke, and K. Schulten, VMD: visual molecular dynamics, J. Mol. Graph. **14**, 33 (1996).

[36] M.-L. Diebold-Durand, H. Lee, L. B. R. Avila, H. Noh, H.-C. Shin, H. Im, F. P. Bock, F. Bürmann, A. Durand, A. Basfeld, *et al.*, Structure of full-length SMC and rearrangements required for chromosome organization, Mol. Cell **67**, 334 (2017).

[37] F. Bürmann, B.-G. Lee, T. Than, L. Sinn, F. J. O'Reilly, S. Yatskevich, J. Rappsilber, B. Hu, K. Nasmyth, and J. Löwe, A folded conformation of MukBEF and cohesin, Nat. Struct. Mol. Biol. **26**, 227 (2019).

[38] Y. M. Soh, F. Bürmann, H. C. Shin, T. Oda, K. S. Jin, C. P. Toseland, C. Kim, H. Lee, S. J. Kim, M. S. Kong, M. L. Durand-Diebold, Y. G. Kim, H. M. Kim, N. K. Lee, M. Sato, B. H. Oh, and S. Gruber, Molecular basis for SMC rod formation and its dissolution upon DNA binding, Mol. Cell **57**, 290 (2015).

[39] M. Hirano and T. Hirano, Hinge-mediated dimerization of SMC protein is essential for its dynamic interaction with DNA, EMBO J. **21**, 5733 (2002).

[40] A. Chiu, E. Revenkova, and R. Jessberger, DNA interaction and dimerization of eukaryotic SMC hinge domains, J. Biol. Chem. **279**, 26233 (2004).

[41] J. J. Griese, G. Witte, and K. P. Hopfner, Structure and DNA binding activity of the mouse condensin hinge domain highlight common and diverse features of SMC proteins, Nucleic Acids Res. **38**, 3454 (2010).

[42] A. Kurze, K. A. Michie, S. E. Dixon, A. Mishra, T. Itoh, S. Khalid, L. Strmecki, K. Shirahige, C. H. Haering, J. Löwe, and K. Nasmyth, A positively charged channel within the Smc1/Smc3 hinge required for sister chromatid cohesion, EMBO J **30**, 364 (2011).

[43] M. Sun, T. Nishino, and J. F. Marko, The SMC1-SMC3 cohesin heterodimer structures DNA through supercoiling-dependent loop formation, Nucleic Acids Res. **41**, 6149 (2013).

[44] S. Uchiyama, K. Kawahara, Y. Hosokawa, S. Fukakusa, H. Oki, S. Nakamura, Y. Kojima, M. Noda, R. Takino, Y. Miyahara, T. Maruno, Y. Kobayashi, T. Ohkubo, and K. Fukui, Structural Basis for Dimer Formation of Human Condensin Structural Maintenance of Chromosome Proteins and Its Implications for Single-stranded DNA Recognition, J. Biol. Chem. **290**, 29461 (2015).

[45] A. Alt, H. Q. Dang, O. S. Wells, L. M. Polo, M. A. Smith, G. A. McGregor, T. Welte, A. R. Lehmann, L. H. Pearl, J. M. Murray, and A. W. Oliver, Specialized interfaces of Smc5/6 control hinge stability and DNA association, Nat. Commun. **8**, 14011 (2017).

[46] C. Chapard, R. Jones, T. van Oepen, J. C. Scheinost, and K. Nasmyth, Sister DNA entrapment between juxtaposed smc heads and kleisin of the cohesin complex, Mol. Cell **75**, 224 (2019).

[47] J. E. Collier, B. G. Lee, M. B. Roig, S. Yatskevich, N. J. Petela, J. Metson, M. Voulgaris, A. Gonzalez Llamazares, J. Löwe, and K. A. Nasmyth, Transport of DNA within cohesin involves clamping on top of engaged heads by Scc2 and entrapment within the ring by Scc3, Elife **9** (2020).

[48] F. U. Seifert, K. Lammens, G. Stoehr, B. Kessler, and K.-P. Hopfner, Structural mechanism of ATP-dependent DNA binding and DNA end bridging by eukaryotic Rad50, EMBO J. **35**, 759 (2016).

[49] Y. Liu, S. Sung, Y. Kim, F. Li, G. Gwon, A. Jo, A.-K. Kim, T. Kim, O.-k. Song, S. E. Lee, *et al.*, ATP-dependent DNA binding, unwinding, and resection by the Mre11/Rad50 complex, EMBO J. **35**, 743 (2016).

[50] Z. Shi, H. Gao, X. C. Bai, and H. Yu, Cryo-EM structure of the human cohesin-NIPBL-DNA complex, Science **368**, 1454 (2020).

[51] T. L. Higashi, P. Eickhoff, J. S. Sousa, J. Locke, A. Nans, H. R. Flynn, A. P. Snijders, G. Papageorgiou, N. O'Reilly, Z. A. Chen, F. J. O'Reilly, J. Rappsilber, A. Costa, and F. Uhlmann, A Structure-Based Mechanism for DNA Entry into the Cohesin Ring, Mol. Cell **79**, 917 (2020).

[52] E. J. Banigan, A. A. van den Berg, H. B. Brandõ, J. F. Marko, and L. A. Mirny, Chromosome organization by one-sided and two-sided loop extrusion, Elife **9** (2020).

[53] K. W. Muir, Y. Li, F. Weis, and D. Panne, The structure of the cohesin ATPase elucidates the mechanism of SMC-kleisin ring opening, Nat. Struct. Mol. Biol. **27**, 233 (2020).

[54] C. Bouchiat, M. D. Wang, J.-F. Allemand, T. Strick, S. Block, and V. Croquette, Estimating the persistence length of a worm-like chain molecule from force-extension measurements, Biophys. J. **76**, 409 (1999).

[55] J. K. Ryu, S.-H. Rah, R. Janissen, J. W. J. Kerssemkers, and C. Dekker, Resolving the step size in condensin driven DNA loop-extrusion identifies ATP binding as the step-generating process, biorXiv **2020.11.04.368506v1** (2020).

[56] J. Stigler, G. Ö. Çamdere, D. E. Koshland, and E. C. Greene, Single-molecule imaging reveals a collapsed conformational state for DNA-bound cohesin, Cell Rep. **15**, 988 (2016).

[57] H. B. Brandão, P. Paul, A. A. van den Berg, D. Z. Rudner, X. Wang, and L. A. Mirny, RNA polymerases as moving barriers to condensin loop extrusion, Proc. Natl. Acad. Sci. U.S.A. **116**, 20489 (2019).

[58] J. M. Eeftens, A. J. Katan, M. Kschonsak, M. Hassler, L. de Wilde, E. M. Dief, C. H. Haering, and C. Dekker, Condensin Smc2-Smc4 Dimers Are Flexible and Dynamic, Cell Rep. **14**, 1813 (2016).

[59] J.-K. Ryu, A. J. Katan, E. O. van der Sluis, T. Wisse, R. de Groot, C. H. Haering, and C. Dekker, The condensin holocomplex cycles dynamically between open and collapsed states, Nat. Struct. Mol. Biol. , 1 (2020).

[60] B. G. Lee, F. Merkel, M. Allegretti, M. Hassler, C. Cawood, L. Lecomte, F. J. O'Reilly, L. R. Sinn, P. Gutierrez-Escribano, M. Kschonsak, S. Bravo, T. Nakane, J. Rappsilber, L. Aragon, M. Beck, J. L?we, and C. H. Haering, Cryo-EM structures of holo condensin reveal a subunit flip-flop mechanism, Nat Struct Mol Biol **27**, 743 (2020).

[61] R. D. Giuntoli, N. B. Linzer, E. J. Banigan, C. E. Sing, M. O. De La Cruz, J. S. Graham, R. C. Johnson, and J. F. Marko, DNA-segment-facilitated dissociation of Fis and NHP6A from DNA detected via single-molecule mechanical response, J. Mol. Biol. **427**, 3123 (2015).

[62] A. Badrinarayanan, R. Reyes-Lamothe, S. Uphoff, M. C. Leake, and D. J. Sherratt, In vivo architecture and action of bacterial structural maintenance of chromosome proteins, Science **338**, 528 (2012).

[63] K. Zawadzka, P. Zawadzki, R. Baker, K. V. Rajasekar, F. Wagner, D. J. Sherratt, and L. K. Arciszewska, MukB ATPases are regulated independently by the N- and C-terminal domains of MukF kleisin, Elife **7** (2018).

[64] K. V. Rajasekar, R. Baker, G. L. M. Fisher, J. R. Bolla, J. Mäkelä, M. Tang, K. Zawadzka, O. Koczy, F. Wagner, C. V. Robinson, L. K. Arciszewska, and D. J. Sherratt, Dynamic architecture of the Escherichia coli structural maintenance of chromosomes (SMC) complex, MukBEF, Nucleic Acids Res. **47**, 9696 (2019).

[65] S. Plimpton, Fast parallel algorithms for short-range molecular dynamics, J. Comput. Phys. **117**, 1 (1995).

[66] V. V. Rybenkov, N. R. Cozzarelli, and A. V. Vologodskii, Probability of DNA knotting and the effective diameter of the DNA double helix, Proc. Natl. Acad. Sci. U.S.A. **90**, 5307 (1993).